Deformable and conformal silk hydrogel inverse opal

Kyungtaek Min[a,1], Sookyoung Kim[a,1], and Sunghwan Kim[a,b,2]

[a]Department of Energy Systems Research, Ajou University, Suwon 16499, Republic of Korea; and [b]Department of Physics, Ajou University, Suwon 16499, Republic of Korea

Photonic crystals (PhCs) efficiently manipulate photons at the nanoscale. Applying these crystals to biological tissue that has been subjected to large deformation and humid environments can lead to fascinating bioapplications such as in vivo biosensors and artificial ocular prostheses. These applications require that these PhCs have mechanical durability, deformability, and biocompatibility. Herein, we introduce a deformable and conformal silk hydrogel inverse opal (SHIO); the photonic lattice of this 3D PhC can be deformed by mechanical strain. This SHIO is prepared by the UV cross-linking of a liquid stilbene/silk solution, to give a transparent and elastic hydrogel. The pseudophotonic band gap (pseudo-PBG) of this material can be stably tuned by deformation of the photonic lattice (stretching, bending, and compressing). Proof-of-concept experiments demonstrate that the SHIO can be applied as an ocular prosthesis for better vision, such as that provided by the *tapeta lucida* of nocturnal or deep-sea animals.

silk fibroin | photonic crystal | photo–cross-linking | ocular prosthesis | intraocular pressure sensor

Three-dimensional photonic crystals (3D PhCs), also known as "opals," prepared by the self-assembly of colloidal crystals and their derivatives, have broad applicability in colorimetric sensors, full-color displays, and photonic pigments (1–4). Interferences between strongly scattered waves lead to a modification of the photon density of states in particular energy regions (5). Light waves in these energy regions are also efficiently reflected; this phenomenon is known by different names, such as opalescence, structural color, and photonic band gap. Creatures in nature have evolved to exploit the properties of PhCs, with examples including antireflective nipple arrays in compound eyes, and 3D cuticle PhCs for broad-angle reflection that many scientists have been trying to mimic (6, 7). For biomedical application, artificial biomimetic PhCs are potentially useful as ocular prostheses or highly sensitive biosensors. This sphere of application can be expanded through the use of biocompatible materials with reliable biointerfaces to flexible and deformable tissue (8, 9).

Silk fibroin, derived from the *Bombyx mori* cocoon, is a biocompatible and biodegradable polymer with no toxic or immunogenic properties (10). Recently, optical clarity and good processability have reinvented silk as a material for high-technology, biooptical elements such as lenses, lasers, PhCs, and plasmonic resonators (11–18). Due to the combination of favorable material traits, silk shows promise for use in optical elements for biomedical application. Here we introduce a stretchable, bendable, compressive, and conformal silk hydrogel inverse opal (SHIO) that exhibits structural color even under the mechanical deformation conditions (Fig. 1*A*) to which the biological tissue is subjected. The pseudophotonic band gap (PBG), corresponding to the exhibited structural color, can be precisely tuned by applying mechanical forces to induce deformation of the photonic lattice. Meanwhile, silk is under scrutiny to work in contact with a delicate organ such as the eye. For example, silk was used to engineer corneal epithelium (19) and stroma (20) in vitro. In vivo responses of silk films to rabbit cornea models were also investigated (21). In that sense, we show potential of the SHIO as an ocular prosthesis to improve vision in a similar way to that of the *tapetum lucidum* of nocturnal or deep-sea animals (Fig. 1*B*) (22, 23).

To fabricate the SHIO, layers of submicrometer poly(methyl methacrylate) (PMMA) spheres, with a 300-nm diameter, were stacked in a face-centered cubic (fcc) structure on a silicon substrate, as shown in Fig. 1*C* (12). An aqueous solution of silk fibroin and stilbene was poured into the PMMA template, which was subsequently cross-linked by short-wavelength UV (UVC) light from a low-pressure UV lamp. The low hazard stilbene chromophore, which had already been used as a gain material in a silk laser (13), was chosen as the dopant for the photo–cross-linking of the silk molecules. UVC light induces $[2\pi + 2\pi]$ cycloadditions between the stilbene units, whereas the radicals generated in the silk tethers undergo dityrosine bonding (for details, see *Supporting Information* and Fig. S1) (24, 25). The rate of photo–cross-linking is increased by the aromaticity of the side chain that silk possesses in abundance. Consequently, stilbene can be a good cross-linker for silk fibroin (24, 26). We found that a solution containing 0.02 M of stilbene led to the most rapid rate of cross-linking. To generate the inverse opal structure, the solidified silk film was detached from the silicon substrate and immersed in acetone to dissolve the PMMA spheres. The remaining stilbene was washed out with water over a day. Fig. 1*D* shows the opalescence of the SHIO caused by the diffraction of incident light induced by the periodic silk lattice (Fig. 1*E*). The sky-blue opalescence observed in air changed to red opalescence when the SHIO was immersed in water, because the effective refractive index (RI) increased as the SHIO structure became swollen. In addition, mechanical properties of the SHIO and the bulk silk hydrogel film, both swollen and elastic, were investigated (Fig. S2 and Table S1). In the fabrication process, the

Fig. 1. Deformable SHIO. (*A*) Conceptual images showing deformations (stretchable, bendable, compressive, and conformal) of SHIOs. All SHIOs exhibited red opalescence corresponding to their pseudo-PBG. (*B*) Photograph showing brilliant opalescence of the SHIO attached under a glass bead. Analogous phenomena can be found in nocturnal animals with superior night vision. (*C*) Fabrication steps for the deformable SHIO. A PMMA opal is generated on a silicon substrate. A silk fibroin solution mixed with the stilbene chromophore infiltrates the PMMA opal and then is cured by UVC light from a low-pressure UV lamp. The remaining PMMA spheres are dissolved in acetone. The generated SHIO is immersed in water to wash out the remaining stilbene. (*D*) Photograph taken under white-light illumination in air (*Left*) and water (*Right*), showing clear changes in opalescence. (*E*) SEM image of the SHIO. (Scale bar, 500 nm.)

minimum UV-exposure time required for the stable SHIO was 2 h. The elastic modulus of the silk hydrogel film was increased (more rigid), along with the reduced elastic deformation range, when the UV-exposure time increased. And, we observed that the elastic modulus of the SHIO was smaller than that of the bulk silk hydrogel film due to porosity of the SHIO (more elastic) (27). The elastic deformation range of the SHIO was 10%, similar to bulk, and the optical response was significantly weakened at strains greater than the elastic range (Fig. S3).

Fig. 2*A* shows the spectral responses of reflected light, measured using an optical setup under white-light illumination. By increasing the effective RI, the wavelength corresponding to the photonic mode becomes red-shifted. Immersing the SHIO in isopropyl alcohol (IPA) ($n \sim 1.37$), which is volatile enough not to cause any swelling of the silk matrix, red-shifts the reflection peak (λ_{peak}) from 500 in air to 616 nm (12). However, when the SHIO is immersed in water, the situation becomes more complex because the silk matrix accommodates water molecules and therefore becomes structurally expanded, resulting in a reduced RI. This figure can be qualified theoretically by calculating the pseudo-PBG associated with the lattice geometry and the RI. To identify the lattice constant a (= $\sqrt{2}d$, where d is the void diameter) of the fcc inverse opal, we compared the calculated

photonic band structures and the measured reflectance spectra. As shown in Fig. 2*B*, the calculated pseudo-PBG frequencies (a/λ_{peak}) for the SHIOs in air and IPA are in good agreement with those obtained experimentally when d is 270 nm. The contracted lattice originates from the prolonged exposure to acetone used for removing PMMA spheres (12). To estimate the optical response of the swollen SHIO (in water), we first investigated the RI value of the swollen silk film (Fig. S4). To that end, a He–Ne laser beam was refracted at the boundary between air and the swollen silk film; the RI value of the silk film, obtained according to Snell's law, was observed to reduce from 1.54 to 1.43. As a consequence, a theoretical calculation estimates that the silk matrix in the swollen SHIO is expanded by 3% (270 to 278 nm in d), making the silk film elastic.

To evaluate the spectral response to stretching, the SHIO was double-banked, using clamps, during the collection of the reflected spectra, as shown in Fig. 3*A*. The λ_{peak} of the reflected signal was plotted as a function of mechanical strain, defined as $\Delta L/L$ (L: the length of the silk film, ΔL: the elongated length of the silk film). As shown in Fig. 3*B*, a strain of 10% induces a 7-nm blue shift of λ_{peak}. The Bragg–Snell (vertical incident) diffraction equation, $\lambda_{peak} = 2n_{eff}d$, where n_{eff} is the effective RI and d is the interplanar spacing, indicates that the observed spectral response
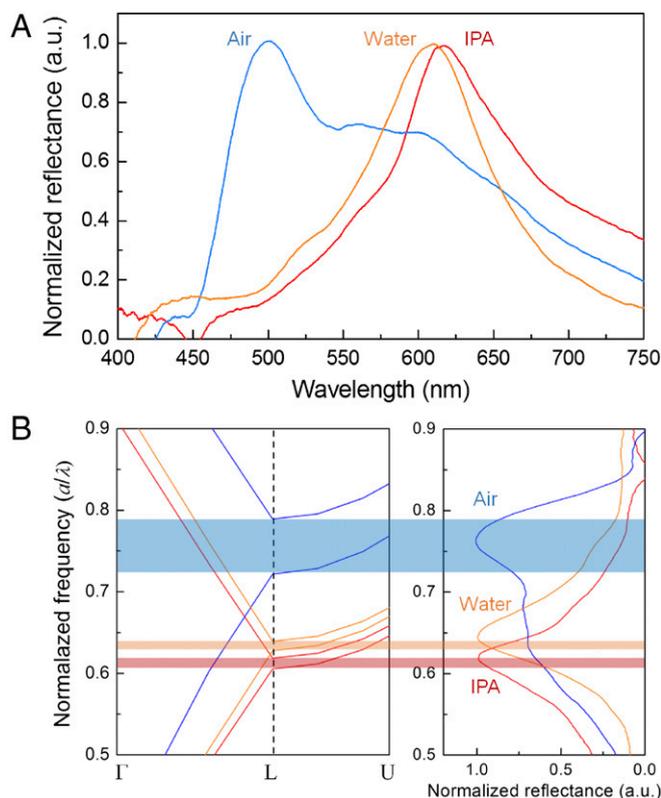
Fig. 2. Optical response of the SHIO. (*A*) Measured reflectance spectra of the SHIO. The reflectance peak is red-shifted when water and IPA infiltrate the SHIO. (*B*) Photonic band structures of the SHIO in air (blue), water (orange), and IPA (red), calculated using the PWE method. Unlike immersion in IPA, water molecules are absorbed into the SHIO, which then expands its structure, resulting in a reduced refractive index of the silk matrix.

is not the result of the elongated (*x* direction) stretching of the lattice, but is due to the simultaneously contracted interplanar distance perpendicular to the film surface (*z* direction) (28, 29). We performed numerical simulations, using a finite-difference time-domain (FDTD) method, to examine the effect of the lattice constant on the pseudo-PBG of the SHIO (Fig. S5). The FDTD results indicate that the reflection peak, corresponding to the pseudo-PBG, is highly sensitive to the interplanar distance, whereas the stretched interparticle space in the *x*- and *y*- directions does not appear to influence the pseudo-PBG. In addition, the Poisson ratio (υ) of the SHIO can be estimated from simulated and experimental values using the equation $\varepsilon_z = -\upsilon\varepsilon_x$, where ε_z ($\varepsilon_x = \Delta L/L$) is the mechanical strain in the *z* direction (*x* direction) (28). We obtained a value of $\upsilon = 0.12$. This value is smaller than those reported for nonporous elastomers ($\upsilon \sim 0.5$) (30). In porous polymers, however, to maintain a constant volume, a compression in one direction is not required to be accompanied by an expansion in perpendicular directions (29). Fig. 3*C* demonstrates the response of the λ_{peak} to repeated stretch and release steps (10% strain) over three cycles (the maximum number of cycles without loss in optical quality). The blue-shifted peak observed under stretching was fully recovered when the stress was relaxed, showing the flexibility and durability of the SHIO.

As a direct way to alter the interplanar spacing, weights were loaded to apply uniform pressure onto the SHIO (Fig. 4*A*). The applied pressure decreases interplanar spacing, thereby blue-shifting the pseudo-PBG (Fig. 4*B*). The sensitivity of the SHIO to a pressure of 0.25 nm/kPa, obtained from the plot, is comparable to that of a polyacrylamide-hydrogel inverse opal (31).

Although the detection limit is relatively low compared with electrical-based pressure sensors (32, 33), it is sufficient for the detection of physiological signals such as intraocular pressure, while providing the biofriendly features and the wireless detection capability that electrical devices cannot provide (34).

As technology advances, more high-technological devices begin to blend with our biological systems for improving or recovering biological functions (8, 35–37). A technologically relevant application of the deformable and conformal SHIO is the improvement of human or animal vision. Nocturnal and deep-sea animals have the advantage of a *tapetum lucidum*, which is a layer of tissue consisting of regularly arranged collagen fibers (22, 23). The *tapetum lucidum* can be regarded as a protein-based PhC (like the SHIO) and therefore visible light can be reflected by the *tapetum* and returned through the retina to increase the light available to the photoreceptors, providing superior night vision. As proof-of-concept, we investigated the optical properties of the SHIO on the curved surface of an eye model. Hemispheres of agarose gel and soft contact lenses were used in this eye model because the gels were tissue equivalent and easily prepared in any shape (38–40). Especially, translucency of agarose gel made it easier to observe the light path traveled through
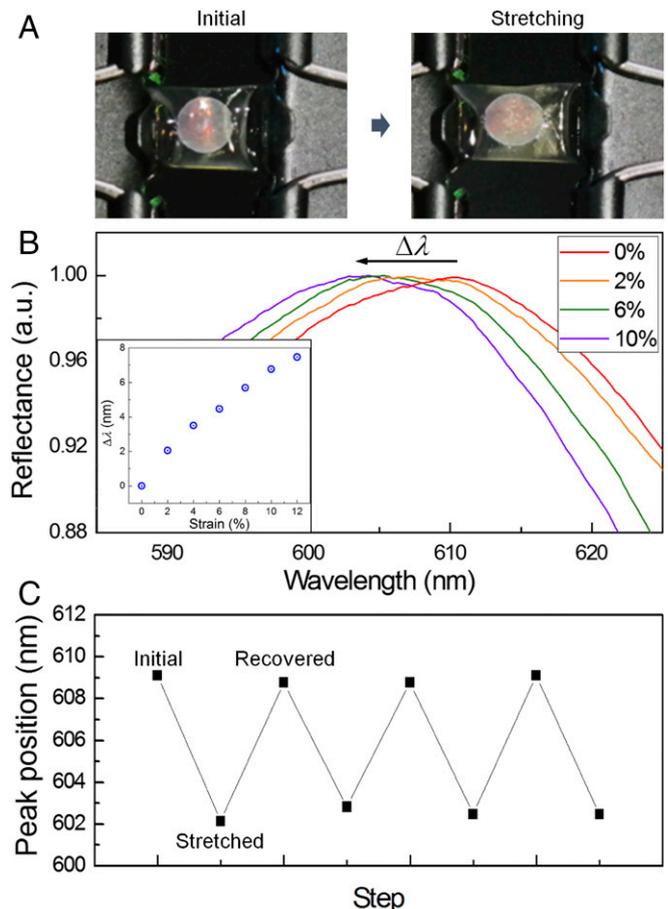
Fig. 3. Optical response of the SHIO film to stretching. (*A*) Photographic images taken under the application of tension to the SHIO. (*B*) Reflection spectra showing the blue shift in the pseudo-PBG owing to stretching. Elongation of the SHIO sheet induces contraction of the interplanar space in the vertical direction, thereby blue-shifting the reflection peak. (*Inset*) Plot of the wavelength shifts of the reflection peak as a function of strain. (*C*) The stretching–recovering cycling of the peak wavelength position when the SHIO is subjected to 10% strain. There is no deterioration in reflection properties for up to three cycles.

Min et al.
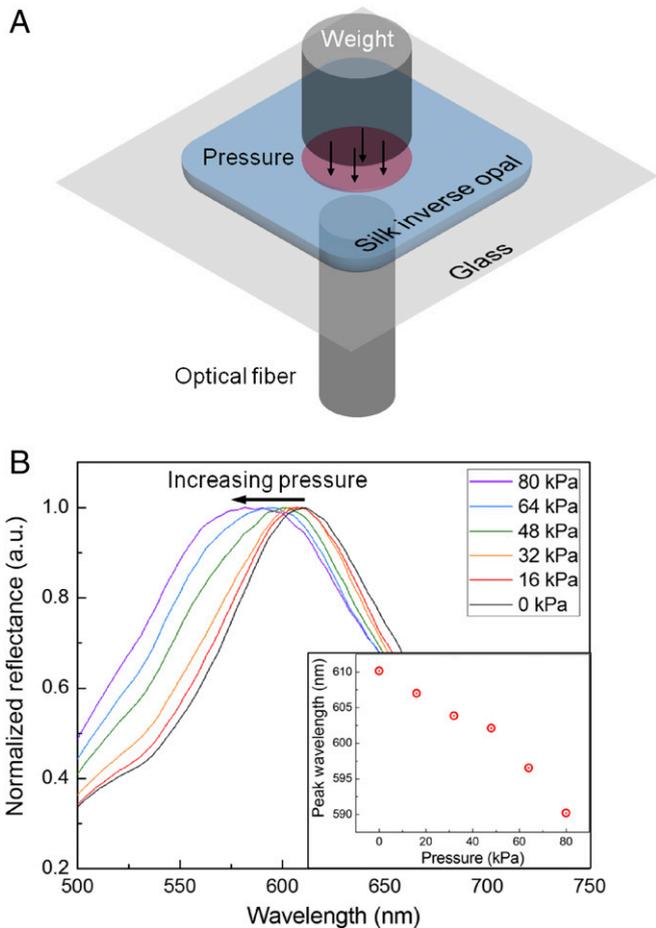
Fig. 4. Optical response of the SHIO on compression. (*A*) Schematic diagram showing how the optical response of the SHIO under pressure is measured. To induce compression, weights of the same diameter as the SHIO were loaded onto the SHIO. (*B*) Relationship between peak positions and compressive pressures. The plot shows the blue shift of the reflection peak with increasing pressure due to reduction of the interplanar space. (*Inset*) Plot of peak wavelength as a function of pressure.

the gel. The photographs in Fig. 5*A* show propagating red laser beams through hemispheric gels containing silk films (with and without the SHIO) on the top of the gel. Because the SHIO is conformally attached onto the curved gel, it can be considered to be a concave mirror surface, as simulated in Fig. 5*B*; the partially reflected red laser beam is focused at the focal point [$f = -(1/2)r_0$ where f is the focal length and r_0 is the radius of the sphere]. Additionally, the accumulated light, originating from the strongly scattered light, can be observed at the boundary between the agarose gel and the SHIO. This indicates that incident light can be efficiently absorbed by photoreceptors placed in front of the SHIO.

To confirm this light enhancement, we investigated the absorption of a blue dye (gardenia blue) solution inserted into the contact lens at the point where the silk film (with or without the SHIO) is located behind the contact lens (Fig. 5*C*). The blue color of the dye originates from its broad-band absorption properties that range from green to red ([Fig. S6](#)), and is suitable for the SHIO exhibiting red reflective color. Fig. 5*D* shows that the inserted SHIO enhances the absorption of incident white light in the broad range of 510–660 nm. It is especially interesting that the maximal absorption enhancement (with a factor of ~1.3) is obtained at ~600 nm, close to that of the pseudo-PBG of the SHIO. This result indicates that the light reflected by the SHIO

was reabsorbed by the dye solution. In addition, if the contact lens is regarded to be an optical waveguide, the optical loss caused by the curvature of the waveguide is reduced by the SHIO, which recouples the leaked light back into the waveguide ([Fig. S7](#)). It is noteworthy that the realized SHIO is an example of the artificial *tapetum lucidum* totally mimicking the natural one (protein-based and elastic PhC). Although it is necessary to verify these optical functionalities in a real biological system, the conformability and the biofriendly properties of the SHIO may lead to an artificial *tapetum* for better visual acuity in low light ([Fig. S8](#)).

The detection of intraocular pressure (IOP), the main indicator of glaucoma, is a considerably promising application of the deformable SHIO (34). The underlying principle of noninvasive IOP sensors relies on converting changes in the curvature of the cornea into detectable signals such as capacitance and strain. To investigate the effects of curvature on the optical response of the SHIO, we inserted an SHIO between a contact lens and an agarose gel hemisphere (Fig. 5*E*). As shown in Fig. 5*F*, a 5-nm red shift of the reflection peak was obtained when the curvature was reduced by two-thirds ($1/2$ cm^{-1} to $1/3$ cm^{-1}). In measurements of optical structure on a curved surface, structural variations associated with the surface curvature must be considered because an incident light beam has a finite area of illumination. In effect, the averaged incident angle becomes smaller as the curvature of the SHIO is reduced, resulting in a red shift of the spectrum of the collected reflection signal. The FDTD simulation also exhibited a red-shifted spectrum for the smaller curvature, in good agreement with the experimental result (Fig. 5*F*). To apply the SHIO as the indicator for glaucoma, we should be able to detect about 3% change in the radius of curvature (41), corresponding to subnanometer deviation of the pseudo-PBG wavelength. This detection requires highly resolute spectrometry, relatively expensive but certainly available in the medical industry. Through the proof-of-concept experiment, we quantitatively investigated the operation of the SHIO on the eye-like spherical surface and computationally analyzed the optical response, which may be useful for ophthalmology inspection.

For in vivo and in vitro applications of the SHIO, investigation on the biodegradability is important to predict the lifetime of the device. Using the biodegradation evaluation method described in refs. 42 and 43, we could confirm that the UV-cross-linked silk hydrogel film exhibited the slower degradation rate than those of other reported water-insoluble silk films ([Fig. S9](#)), which could lead to implantable devices with long-term degradation (42, 43). It is noteworthy that the transparency of the silk films was well preserved during the biodegradation process ([Fig. S10](#)).

In conclusion, deformable and conformal silk inverse opals have been produced via photo–cross-linking of the stilbene chromophore with silk molecules under UVC exposure. Forces applied to induce deformations such as stretching, compression, and flection can be used to precisely tune the pseudo-PBG, and the corresponding structural color of the SHIO. When the SHIO is conformally placed on the curved surface of an agarose gel hemisphere, an artificial model of the eye, the incident light accumulates at the boundary between the SHIO and the gel hemisphere, along with the focused, reflected light. The attached SHIO also enhances the absorption of a blue dye solution by increasing the optical path length. We expect that this SHIO may be applicable as an artificial *tapetum*, to help improve human night vision to see as nocturnal animals do. In addition, changes in the pseudo-PBG position with curvature may provide a way to detect IOP. By exploiting the favorable material traits of silk, our deformable silk-based photonic nanostructure adds a dimension at the interface between nanooptics and biology.

Methods

Silk Fibroin Solution Preparation. *B. mori* cocoons were boiled for 30 min in an aqueous solution of 0.02 M sodium carbonate (Na$_2$CO$_3$) and then rinsed

Min et al.

www.manaraa.com
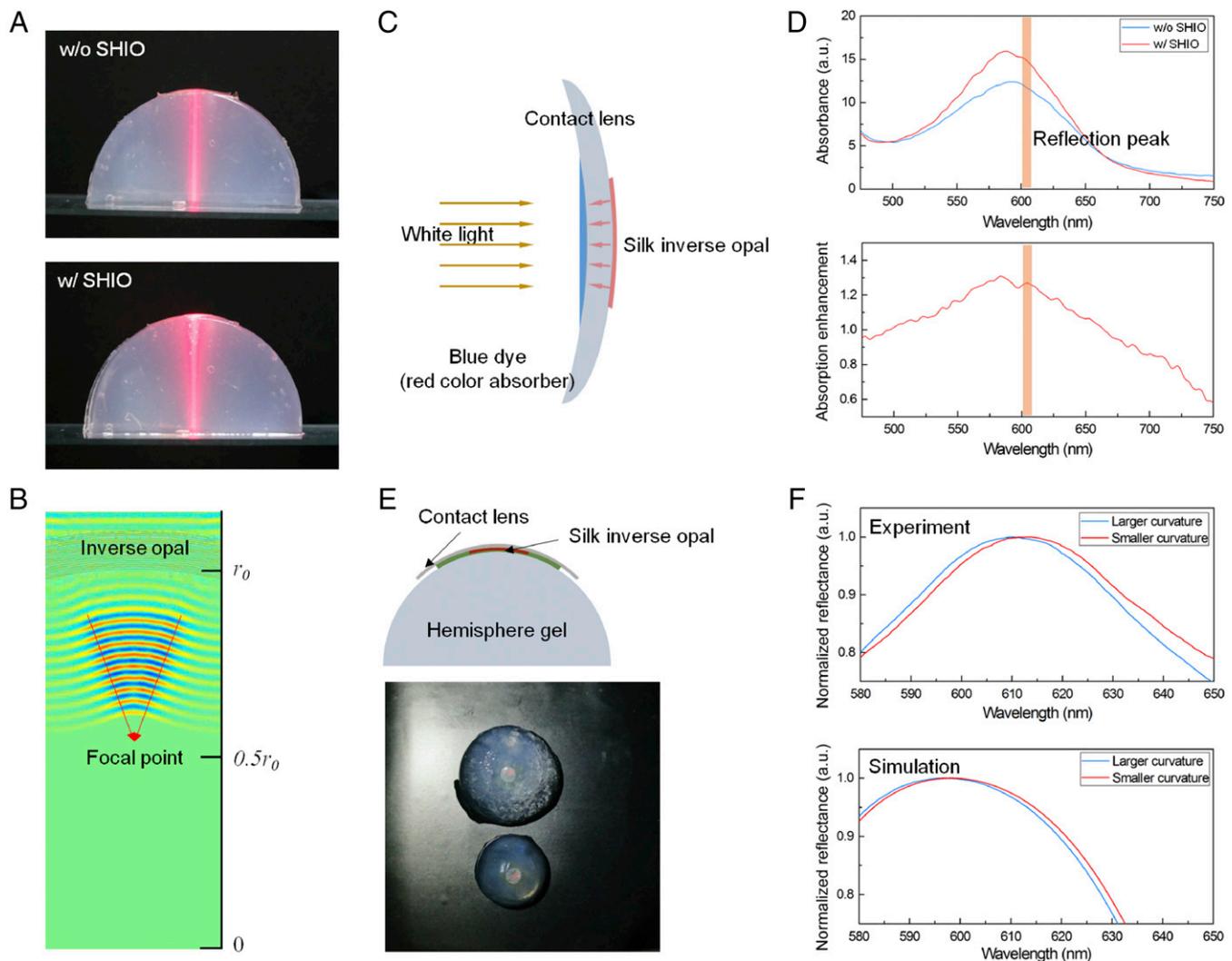
Fig. 5. Proof-of-concept experiment for artificial ocular prostheses. (*A*) Photographic images showing the reflection behavior of a red laser beam in the SHIO conformally placed on an agarose gel hemisphere (an artificial eye model). Scattered light partly accumulates at the boundary between the SHIO and the agarose gel, while some is reflected in the backward direction. The FDTD simulation in *B* reveals that the conformal SHIO acts as a concave mirror, focusing the reflected light. The concept can be applied to an artificial *tapetum* for better human night vision and is related to the better absorption of incident light by photoreceptors by the artificial *tapetum* reflector. (*C* and *D*) Schematic diagram and absorption measurement of a proof-of-concept experiment to prove better absorption of incident light by the SHIO. Absorption enhancement factors were also plotted. (*E* and *F*) Optical response of the SHIO on agarose gels with different curvatures related to the IOP. On the smaller curvature (larger IOP), the SHIO exhibits the red-shifted reflection peak in experiment (*Top*) and simulation (*Bottom*).

with distilled water and dried for 24 h to remove sericin proteins. The extracted silk fibroin was then dissolved in a 9.3 M lithium bromide solution and incubated at 60 °C for 4 h, to yield a 20 wt % solution. This solution was dialyzed against distilled water using a dialysis membrane (Cellu-Sep T1, Membrane Filtration Products, MWCO 3.5K) at room temperature for 48 h. The dialysate was centrifuged twice for 20 min at −1 °C at 9,000 rpm, to remove impurities. The final concentration of silk fibroin aqueous solution was ∼8 wt %.

SHIO Fabrication Process. Commercially available PMMA spheres (2% concentration dispersed in water, MMA300, Phosphorex) were used to generate a template for a silk inverse opal. A 5 μL sample of the PMMA solution was dropped onto a silicon substrate and then heated on a hotplate at 70 °C to vaporize water and generate the self-assembled PMMA opal. A silk solution containing the stilbene chromophore (Stilbene 420, Exciton) was then infiltrated into the PMMA opal. The silk solution was then cross-linked using UVC radiation from a low-pressure UV lamp (G36T5VH, Serve Tool Inc.) for 2 h. The lamp emits both 185- and 254-nm UV light at 40 W. The cured silk film was detached from the silicon wafer and immersed in acetone for 24 h to remove the PMMA spheres. The generated silk inverse opal structure was

rinsed with IPA and dried using a nitrogen gun. When soaked in water, the silk inverse opal forms an elastic hydrogel inverse opal.

Optical Measurements. Optical properties of the SHIOs were characterized using a vis/near-infrared fiber-optic spectrometer (USB-2000, Ocean Optics). For the measurement of reflectance spectra, a 1 × 2 fiber coupler enables white light to be fed to the sample, while simultaneously capturing the reflected signal. The reflected optical signal was directly fed into the spectrometer through a fiber. Spectral responses under mechanical strain were measured using a spectrometer as described above, and changes in structure were induced by increasing weight in defined amounts, at regular intervals, or by the use of a clip on both sides of the sample.

Fabrication of Biomimetic Eye Models. The curved surface of the eye was modeled using an agarose gel. A hemispherical agarose gel was made by mixing a solution of 2 wt % aqueous sodium alginate with 1 wt % aqueous calcium chloride solution followed by pouring into a hemispherical framework. The mixture was dried for 24 h, resulting in a hemispherical gel. For the enhancement of the light absorption experiments, a soft contact lens was used. An aqueous solution of natural gardenia blue dye was dropped onto

Min et al.

the concave surface of the contact lens, whereas the SHIO was attached to the convex surface.

Numerical Simulations. The photonic band diagrams for the inverse opals with the fcc structure were simulated using the commercial software (BandSOLVE, Rsoft Design Group) that implements the plane-wave expansion (PWE) code. In the PWE simulation, a convergence tolerance of 10^{-8} was used to obtain eigenvalue frequencies. The refractive indices of water, IPA, the silk film, and the swollen silk film were assumed to be 1.33, 1.37, 1.54, and 1.43, respectively. FDTD simulations were performed using a commercial software package (FDTD Solutions, Lumerical Solutions). To estimate the pseudo-PBG wavelength of the inverse opal structure, reflectance spectra of the inverse opal structures in the L-point direction were calculated. Perfect matching layers were applied at the boundaries in the propagation direction of the plane-wave source (z axis), whereas the

boundary conditions in the other directions were set to be periodic (x and y axes). The refractive indices of these materials were also assumed to be constants, as mentioned above.

Silk Degradation. Silk hydrogel films were incubated at 37 °C in 20 mL PBS solutions which contained 0.23 U/mL protease XIV (Sigma-Aldrich) at pH 7.2. Each solution contained an ∼20 mg amount of silk films. After the incubation, the samples were rinsed in distilled water and dried on the 50 °C hotplate for 30 min. Then, weights of degraded silk hydrogels were measured every hour.

1. Blanco A, et al. (2000) Large-scale synthesis of a silicon photonic crystal with a complete three-dimensional bandgap near 1.5 micrometres. *Nature* 405:437–440.
2. Arsenault AC, Puzzo DP, Manners I, Ozin GA (2007) Photonic-crystal full-color displays. *Nat Photonics* 1:468–472.
3. Honda M, Kataoka K, Seki T, Takeoka Y (2009) Confined stimuli-responsive polymer gel in inverse opal polymer membrane for colorimetric glucose sensor. *Langmuir* 25:8349–8356.
4. Aguirre CI, Reguera E, Stein A (2010) Colloidal photonic crystal pigments with low angle dependence. *ACS Appl Mater Interfaces* 2:3257–3262.
5. Joannopoulos JD, Villeneuve PR, Fan S (1997) Photonic crystals: Putting a new twist on light. *Nature* 386:143–149.
6. Vukusic P, Sambles JR (2003) Photonic structures in biology. *Nature* 424:852–855.
7. Kreysing M, et al. (2012) Photonic crystal light collectors in fish retina improve vision in turbid water. *Science* 336:1700–1703.
8. Humar M, et al. (2016) Toward biomaterial-based implantable photonic devices. *Nanophotonics* 5:60–80.
9. Nizamoglu S, et al. (2016) Bioabsorbable polymer optical waveguides for deep-tissue photomedicine. *Nat Commun* 7:10374.
10. Omenetto FG, Kaplan DL (2010) New opportunities for an ancient material. *Science* 329:528–531.
11. Tao H, et al. (2012) Implantable, multifunctional, bioresorbable optics. *Proc Natl Acad Sci USA* 109:19584–19589.
12. Kim S, et al. (2012) Silk inverse opals. *Nat Photonics* 6:818–823.
13. Toffanin S, et al. (2012) Low-threshold blue lasing from silk fibroin thin films. *Appl Phys Lett* 101:091110.
14. Jung H, Min K, Jeon H, Kim S (2016) Physically transient distributed feedback laser using optically activated silk bio-ink. *Adv Opt Mater* 4:1738–1743.
15. Amsden JJ, et al. (2010) Rapid nanoimprinting of silk fibroin films for biophotonic applications. *Adv Mater* 22:1746–1749.
16. Kim S, et al. (2014) All-water-based electron-beam lithography using silk as a resist. *Nat Nanotechnol* 9:306–310.
17. Tao H, et al. (2010) Metamaterial silk composites at terahertz frequencies. *Adv Mater* 22:3527–3531.
18. Lee M, Jeon H, Kim S (2015) A highly tunable and fully biocompatible silk nanoplasmonic optical sensor. *Nano Lett* 15:3358–3363.
19. Bray LJ, et al. (2011) Human corneal epithelial equivalents constructed on Bombyx mori silk fibroin membranes. *Biomaterials* 32:5086–5091.
20. Lawrence BD, Marchant JK, Pindrus MA, Omenetto FG, Kaplan DL (2009) Silk film biomaterials for cornea tissue engineering. *Biomaterials* 30:1299–1308.
21. Ghezzi CE, et al. (2016) Degradation of silk films in multipocket corneal stromal rabbit models. *J Appl Biomater Funct Mater* 14:e266–e276.
22. Land MF (1972) The physics and biology of animal reflectors. *Prog Biophys Mol Biol* 24:75–106.
23. Warrant EJ, Locket NA (2004) Vision in the deep sea. *Biol Rev Camb Philos Soc* 79:671–712.
24. Jahnke A, Beile B, Meier H (2011) Photo-cross-linking of polymethacrylates with stilbene chromophores in the side chains. *Helv Chim Acta* 94:2111–2124.
25. Applegate MB, et al. (2016) Photocrosslinking of silk fibroin using riboflavin for ocular prostheses. *Adv Mater* 28:2417–2420.
26. Ravikrishnan A, Sudhakara P, Kannan P (2010) Stilbene-based liquid crystalline and photocrosslinkable polynaphthylphosphate esters. *J Mater Sci* 45:435–442.
27. Xu Y, et al. (2000) Measurement of mechanical properties for dense and porous polymer films having a low dielectric constant. *J Appl Phys* 88:5744–5750.
28. Fudouzi H, Sawada T (2006) Photonic rubber sheets with tunable color by elastic deformation. *Langmuir* 22:1365–1368.
29. Arsenault AC, et al. (2006) From colour fingerprinting to the control of photoluminescence in elastic photonic crystals. *Nat Mater* 5:179–184.
30. Nielsen LE (1970) Generalized equation for the elastic moduli of composite materials. *J Appl Phys* 41:4626–4627.
31. Wang J, Cao Y, Feng Y, Yin F, Gao J (2007) Multiresponsive inverse-opal hydrogels. *Adv Mater* 19:3865–3871.
32. Pan L, et al. (2014) An ultra-sensitive resistive pressure sensor based on hollow-sphere microstructure induced elasticity in conducting polymer film. *Nat Commun* 5:3002.
33. Takei K, et al. (2010) Nanowire active-matrix circuitry for low-voltage macroscale artificial skin. *Nat Mater* 9:821–826.
34. Farandos NM, Yetisen AK, Monteiro MJ, Lowe CR, Yun SH (2015) Contact lens sensors in ocular diagnostics. *Adv Healthc Mater* 4:792–810.
35. Kim DH, Ghaffari R, Lu N, Rogers JA (2012) Flexible and stretchable electronics for biointegrated devices. *Annu Rev Biomed Eng* 14:113–128.
36. Humayun MS, et al.; Argus II Study Group (2012) Interim results from the international trial of Second Sight's visual prosthesis. *Ophthalmology* 119:779–788.
37. Stingl K, et al. (2013) Artificial vision with wirelessly powered subretinal electronic implant alpha-IMS. *Proc R Soc B-Biol Sci* 280:20130077.
38. Appleby A, Leghrouz A (1991) Imaging of radiation dose by visible color development in ferrous-agarose-xylenol orange gels. *Med Phys* 18:309–312.
39. Holligan DL, Gillies GT, Dailey JP (2003) Magnetic guidance of ferrofluidic nanoparticles in an *in vitro* model of intraocular retinal repair. *Nanotechnology* 14:661–666.
40. Maxwell AD, et al. (2010) A tissue phantom for visualization and measurement of ultrasound-induced cavitation damage. *Ultrasound Med Biol* 36:2132–2143.
41. Wang W, Du S, Zhang X (2015) Corneal deformation response in patients with primary open-angle glaucoma and in healthy subjects analyzed by Corvis ST. *Invest Ophthalmol Vis Sci* 56:5557–5565.
42. Jin H-J, et al. (2005) Water-stable silk films with reduced β-sheet content. *Adv Funct Mater* 15:1241–1247.
43. Lu Q, et al. (2011) Degradation mechanism and control of silk fibroin. *Biomacromolecules* 12:1080–1086.
44. Stuber FA, Ulrich H, Rao DV, Sayigh AAR (1969) Photocrosslinking of stilbene-modified polymers. *J Appl Polym Sci* 13:2247–2255.
45. Jeon EY, et al. (2015) Rapidly light-activated surgical protein glue inspired by mussel adhesion and insect structural crosslinking. *Biomaterials* 67:11–19.
46. Smith DR, Pendry JB, Wiltshire MCK (2004) Metamaterials and negative refractive index. *Science* 305:788–792.
47. Walheim S, Schäffer E, Mlynek J, Steiner U (1999) Nanophase-separated polymer films as high-performance antireflection coatings. *Science* 283:520–522.
48. Ollivier FJ, et al. (2004) Comparative morphology of the tapetum lucidum (among selected species). *Vet Ophthalmol* 7:11–22.

Min et al.

www.manaraa.com